Influence of Trailing-edge Thickness of Nozzle End on Flow-induced Noise Investigated by DNS

Vitor Gabriel Kleine, vitorkleine@gmail.com
Marcos Aurélio Ortega, ortega@ita.br
Bento Silva de Mattos, bmattos@ita.br
Instituto Tecnológico de Aeronáutica, Divisão de Engenharia Aeronáutica, Praça Marechal Eduardo Gomes, 50, Vila das Acácias, São José dos Campos - SP, Brazil

Andreas Babucke, babucke@iag.uni-stuttgart.de
Markus J. Kloker, kloker@iag.uni-stuttgart.de
Universität Stuttgart, Institut für Aerodynamik und Gasdynamik, Pfaffenwaldring 21, 70569 Stuttgart, Germany

Abstract. *Sound generation of a subsonic laminar jet has been investigated using two-dimensional direct numerical simulation (DNS). The nozzle end is modeled by a thick flat plate with Mach numbers of $Ma_I = 0.8$ above and $Ma_{II} = 0.2$ below the splitter plate. Two plates with distinct thickness were simulated and the results were compared to a thin plate simulation performed earlier by Babucke, Kloker and Rist. Behind the nozzle end a combination of wake and mixing layer develops. Some mechanisms of noise emission were identified, namely, the vortex emission and the vortex pairing. Broadband noise is emitted and the sound levels at the far-field are approximately the same for all thickness, but some peculiarities on the amplitude spectrum of the acoustic pressure can be noted.*

Keywords: *Direct Numerical Simulation, Aeroacoustic, Trailing-edge, Mixing Layer, Linear Stability Theory*

1. INTRODUCTION

Noise reduction is of special interest for a wide range of technical problems. The current investigation focuses on jet noise as it is a major noise source of aircrafts. The mechanisms of flow-induced sound generation are not yet understood properly. Computational fluid dynamics is an option that can give some insight on that because it solves the problem in the whole domain of interest. Aeroacoustic simulations are relatively new but it has shown potential for developing low-noise technologies. However it demands high requirements in computational performance and accuracy of the scheme. Simulations must be unsteady and the time-step is limited by the resolution in frequency needed. It demands a large computational domain to ensure that all relevant portions of acoustic sources are considered and at the same time high spatial resolution is needed. As the acoustic amplitudes are small compared to the flow-field disturbances, the numerical scheme must be very accurate to minimize spurious numerical sound. The boundary conditions have to be chosen carefully, in order not to spoil the acoustic field with reflections.

Up to now large-eddy or direct numerical simulations of jet noise have been focusing on pure mixing layers (Babucke, Kloker, and Rist, 2008; Colonius, Lele, and Moin, 1997; Bogey, Bailly, and Juve, 2000) or low Reynolds number jets (Freund, 2001), where an S-shaped velocity profile is prescribed at the inflow. Lately the works of Babucke et al. have included the nozzle end modelled by a thin finite plate (Babucke, Kloker, and Rist, 2007b), even proposing a passive 'actuator' for noise reduction (Babucke, Kloker, and Rist, 2007a).

In this two-dimensional DNS, the nozzle end is modelled by a thick plate, being a more realistic approach. Two freestream velocities with respective boundary layers are prescribed on top and below the splitter plate. This leads to a combination of wake and mixing layer behind the plate, and the understanding of the flow mechanisms can help the development of noise reduction technologies. This investigation is a continuation of the works of Babucke et al., therefore the thick plates are compared to the thin plate and some results from Babucke, Kloker, and Rist (2007b) are used. A splitter plate with the same freestream velocity on top and below was simulated as well, to simulate a pure wake, in order to search for similarities.

2. NUMERICAL METHOD

2.1 DNS Code

The DNS (Direct Numerical Simulation) code NS3D developed in the IAG-University of Stuttgart was used. It is a code based on the three-dimensional unsteady compressible Navier-Stokes equations. It is written in conservative formulation, solving for density ρ, the three momentum densities ρu, ρv, ρw and the total energy per unit volume E. The complete set of equations is given in (Babucke et al., 2006).

Temperature dependence of viscosity μ is modeled using the Sutherland law. The Prandtl number $Pr = 0.71$ and the ratio of specific heats $\kappa = 1.4$ are assumed to be constant. The most characteristic parameters describing a compressible

viscous flow are the Mach number Ma and the Reynolds number $Re = \overline{\rho}_\infty \overline{U}_\infty \overline{L}/\overline{\mu}_\infty$, with $\overline{L}$ being a reference length and the overbar denoting dimensional values. Dimensionless quantities are obtained by normalizing time with $\overline{L}/\overline{U}_\infty$, velocities with the inflow velocity $\overline{U}_\infty$, pressure with $\overline{\rho}_\infty \overline{U}^2_\infty$, specific heats with $\overline{L}/\overline{U}^2_\infty/\overline{T}_\infty$ and all other quantities with their respective inflow values.

Spatial discretization in streamwise (x) and normal (y) direction is done by 6^{th}-order compact finite differences. The tridiagonal equation systems of the compact finite differences are solved using the Thomas algorithm. To reduce aliasing error, alternating up- and downwind-biased finite differences are used for the convective terms as proposed by Kloker (1997). The second derivatives are evaluated directly, instead of applying the first derivative twice. This leads to better resolved viscous terms and improves the stability of the code (Babucke, Kloker, and Rist, 2008). Time integration of the Navier-Stokes equations is done using the classical 4^{th}-order Runge-Kutta scheme. More details on the NS3D code can be found in (Babucke et al., 2006).

2.2 Boundary Conditions

The boundary conditions are extremely important for computation of flow-induced noise, and special attention should be taken in order not to spoil the acoustic field with reflections.

For the plate representing the nozzle end wall, an isothermal wall boundary condition is used. The temperature is fixed to its value from the initial condition and the non-slip condition sets the velocity to zero. The pressure is obtained by extrapolation from the interior gridpoints. For the vertical boundary of the plate, the extrapolation is made in order to make the pressure gradient null, since it made the code more stable.

The freestream boundary conditions were based on the methods proposed by Giles (1990). An one-dimensional outflow characteristic boundary condition is used. In order to avoid reflections due to oblique waves an additional damping zone interior to the domain, which forces the variables smoothly to a steady state, was used.

Disturbances obtained from linear stability theory were introduced at the inflow. And an one-dimensional inflow characteristic boundary condition (Giles, 1990) is used to avoid reflections.

The outflow boundary conditions are specially critical, because of the large vortices that should leave the domain and should not contaminate the acoustic field. A combination of grid stretching and spatial low-pass filtering was used in the sponge region. Disturbances become increasingly bad resolved as they propagate downstream and the grid stretches. As the spatial filter depends on the step size in x-direction perturbations are smoothly dissipated before they reach the outflow boundary. This procedure shows very low reflections and has been already applied by Colonius, Lele, and Moin (1993).

2.3 Initial Conditions

The initial condition along the flat plate is obtained from similarity solutions of the boundary-layer equations. The integration of the boundary layer equations further downstream was tried, but due to the nature of the flow, the equations were not suited for the region downstream the nozzle end. Therefore a velocity $\Delta u << 1$ (on the order of 10^{-2}) was added to the steady velocity u, and a temporary grid was created to include points inside the plate, were the resultant velocity was Δu, allowing the downstream integration of the full boundary layer equations. This was done for only a small strip, then the velocity Δu was deducted and the integration continued. The resulting field on the strip where the method was used does not satisfy the Navier-Stokes equations, but using this method it was possible to obtain continuous initial conditions in the whole grid.

2.4 Linear Stability Theory

Linear stability theory (LST) is used to introduce disturbances at the inflow, for further analysis of the flow-field and for understanding the phenomenon.

The amplification rates were obtained using a 4^{th}-order matrix solver combined with Wielandt iteration (inverse iteration). More details on the method can be found in (Babucke, Kloker, and Rist, 2007a).

To introduce disturbances at the inflow the initial condition of the upper boundary layer was used as base flow. According to Fig. 1, a fundamental angular frequency of $\omega = 0.0688$ was chosen for the upper boundary layer, corresponding to the strongest amplified wave.

For further analysis of the flow field using linear stability theory it was necessary to choose a base flow. As the flow is highly unsteady behind the nozzle end, enforcing an artificial steady state does not work properly and since the initial conditions do not satisfy the Navier-Stokes equations behind the plate, the time averaged values of the variables of the resulting field from the DNS simulations are used as base flow. Although the time average values don't satisfy the Navier-Stokes exactly, the linear stability theory was used in the region were the fluctuations are not so large, so the error is believed to be not larger than the error from linearization.

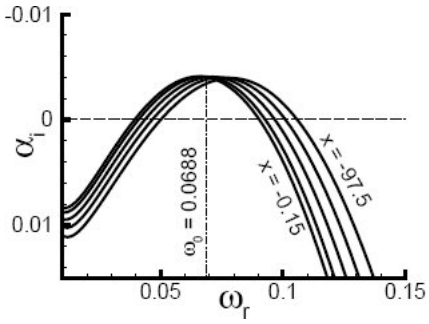

Figure 1. Amplification rates of the upper boundary layer given by linear stability theory for various x-positions along the plate. Source (Babucke, Kloker, and Rist, 2007b).

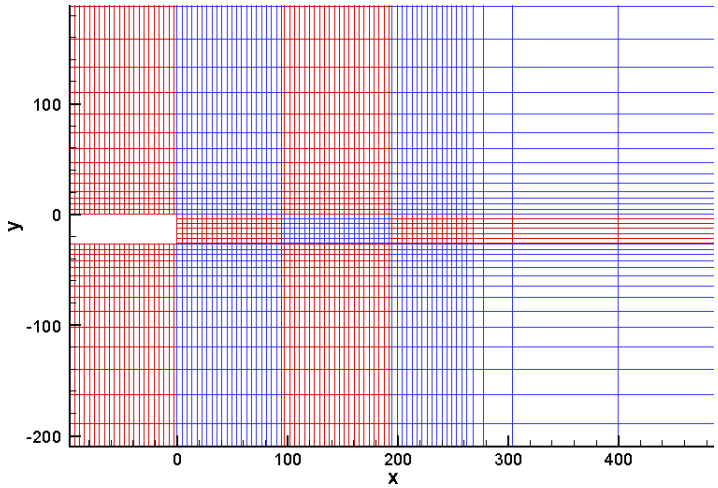

Figure 2. Grid and domain decomposition in x-y plane showing every 30^{th} gridline of 'thicker' case.

3. PARAMETERS

3.1 Flow Parameters

The main purpose of the simulation was to investigate the influence of trailing-edge thickness of a nozzle end. A thin plate has already been simulated (Babucke, Kloker, and Rist, 2007b), therefore two simulations of nozzle end with thick trailing-edge were performed. Behind the nozzle end a combination of wake and mixing layer develops, the results of pure mixing layer are known (Babucke et al., 2006), and then, in search for similarities, a pure wake was also simulated.

For the combination of wake and mixing layer an isothermal subsonic jet with Mach numbers $Ma_I = 0.8$ for the upper and $Ma_{II} = 0.2$ for the lower stream were used and both temperatures were equal, $T_I = T_{II} = 280K$. In the case of the pure wake the parameters of the lower stream are the same as the upper stream ($Ma_I = Ma_{II} = 0.8$). All velocities were normalized by the upper stream velocity U_I and length scales are normalized with the displacement thickness of the fast stream at the inflow, therefore $\delta_{1,I}(x_0) = 1$. The boundary layers of both streams correspond to the same origin of the flat plate.

An isothermal boundary condition at the wall has been chosen. The temperature of the plate is $\overline{T}_{wall} = 296K$, being the mean value of the adiabatic wall temperatures of the streams with $Ma = 0.8$ and $Ma = 0.2$. The Reynolds number $Re = \rho_\infty U_I \delta_{1,I}/\mu_\infty$ is based on the displacement thickness and parameters of the upper stream at the inflow.

The inflow steady parameters are obtained from similarity solutions of boundary layer equations. A single disturbance is introduced at the inflow of the upper boundary layer, with amplitude of $u'_{max} = 0.005$ and the fundamental frequency $\omega_0 = 0.0688$, using the corresponding eigenfunction from the linear stability theory (section 2.4), which is the Tollmien-Schlichting (TS) wave.

3.2 Grid

The cartesian grid is divided into eleven subdomains, four columns in streamwise and three lines in normal direction. The plate is simulated by the absence of a subdomain in the first streamwise position of the middle normal position and the corresponding boundary conditions, as it can be seen in Fig. 2.

The mesh is uniform in streamwise direction up to the sponge region, where the grid is highly stretched to ensure an

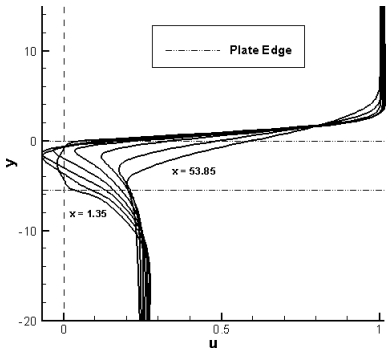

Figure 3. Streamwise velocity profile behind the nozzle end used as base flow for linear stability theory. 'Default' case.

appropriate boundary condition (see 2.2). In the normal direction the middle subdomains present uniform grids and the upper and the lower subdomains present a continuous stretching.

Due to the large ratio of streamwise velocities for the mixing layer, $U_I/U_{II} = 4$, strong instabilities develop behind the nozzle end, so a moderate number of grid points in x-direction is sufficient to simulate the aeroacoustic source. In the pure wake case the ratio of streamwise velocities is small $U_I/U_{II} = 1$, so a higher spatial resolutions appeared to be necessary. The origin of the coordinate system ($x = 0$, $y = 0$) is located on the edge of the plate, the uppermost point of the nozzle end.

'Default' Case The first case is a mixing layer with a plate of thickness $t_K = 5.4$. In order to do the simulation, each middle subdomain contains 650 x 35 points in x- and y- direction, respectively, while each upper and lower subdomain contains 650 x 425 points. The normal direction step size in the middle domain is $\Delta y_{middle} = 0.15$ and up to the sponge region the step size in streamwise direction is $\Delta x = 0.15$.

'Thicker' Case The second case is a mixing layer with a thicker plate, with thickness $t_K = 26.4$. In order to do the simulation, each middle subdomain was changed to contain 650 x 175 points, while the upper and lower subdomains remain the same. The step sizes were not changed.

'Pure Wake' Case The pure wake case was simulated with the same thickness of the 'default' case, a plate of thickness $t_K = 5.4$. In the pure wake case a finer grid was necessary, each middle subdomain contains 1300 x 71 points in x- and y- direction, while each upper and lower subdomain contains 1300 x 849 points. Then the normal direction step size in the middle domain is $\Delta y_{middle} = 0.075$ and up to the sponge region the step size in streamwise direction is $\Delta x = 0.075$.

3.3 Simulation Parameters

In order to ensure that no initial disturbances falsify the results, a number of 90 periods of the fundamental frequency has been computed prior to the results. The sampling rate was 4000 timesteps per period for the combination of mixing layer and wake. For the wake the spatial resolution is greater, hence the time resolution also should be greater, then the sampling rate was 8000 timesteps per period.

For the simulation of the characteristics of the field (results in Sections 4.1 - 4.4) it was computed 16 periods for the 'Default' and 'Pure wake' cases and 32 periods for the 'Thicker' case, because it needed a better resolution in frequency to identify low frequencies near the plate. For the simulation of the pressure disturbances at the far-field (results in Section 4.5) 64 periods were used.

4. RESULTS

4.1 Linear Stability Theory

The time-averaged values of the DNS simulations were used as base flow for the linear stability theory (LST) analyses. This leads to more realistic results than previous works where the base flow is prescribed (Zhuang and Dimotakis, 1995). The base flow velocity u for $t_K = 5.4$ is shown in Fig. 3. Being a combination of a mixing layer and a wake, it is expected to identify two modes of instability, the shear layer mode and the wake mode. Using a thin plate ($t_K = 0.15$), the wake mode couldn't be seen (Babucke, Kloker, and Rist, 2007b), the shear layer mode was the only one identified, as it can be seen in Fig. 4.

For the combination of mixing layer and wake, the amplification rates for several x-positions are shown in Fig. 5. In both simulations the shear layer mode (in red) is dominant, but the wake mode can be seen (in green). For the thicker

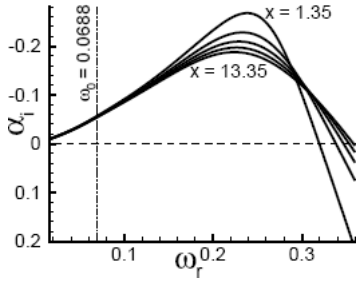

Figure 4. Spatial amplification rates for various x-positions behind the plate predicted by linear stability theory. Thin plate. Source (Babucke, Kloker, and Rist, 2007b).

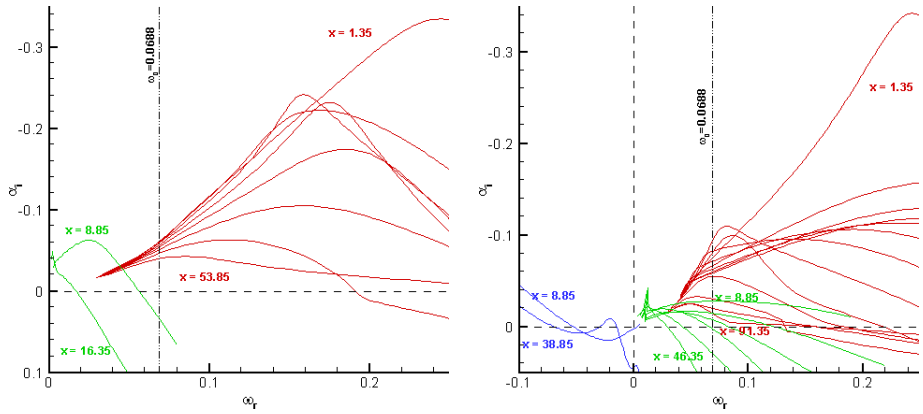

(a) (b)

Figure 5. Spatial amplification rates for various x-positions behind the plate predicted by linear stability theory. Shear layer mode in red, wake mode in green and upstream mode in blue. (a) 'Default' case. (b) 'Thicker' case.

plate ($t_K = 26.4$) the wake mode is amplified further downstream, while for the default thickness ($t_K = 5.4$) the wake mode is amplified only near the plate and for low frequencies. The behavior of the shear layer mode in both cases are similar, being the amplification rate farther downstream greater for the thicker plate.

In the thicker plate there is another unstable mode (in blue) that can be identified, a mode with negative phase-velocity ($\omega/\alpha < 0$), therefore the instability is given by a positive α_i. This mode was obtained only in few x-positions. No disturbances propagating upstream was seen near the plate in the DNS simulation, it is possible that this mode was covered by the other modes or this is merely a theoretical result.

The temporal amplified u'-eigenfunctions for $\alpha = \alpha_r = 0.2$ are shown in Fig. 7 and 8. These are the eigenfunctions found in the first simulation that solves the temporal problem that generates the spatial amplification rates shown in Fig. 5 and 6 (see section 2.4). The position of the plate edges are also shown in the figures.

In the simulations of mixing layer/wake it is possible to identify the shear layer eigenfunction (in red) and the wake eigenfunction (in green). It is clear the similarity between the wake eigenfunctions of the mixing layer/wake and the eigenfunctions of the pure wake. Two eigenfunctions were obtained in the pure wake simulation, one showing disturbance velocity u' concentrated near the edges of the plate and the other showing u' concentrated in the middle of the plate. The former seems to be better related to the wake eigenfunctions of the mixing layer/wake simulations.

4.2 DNS Results

From the DNS simulations of the combination of mixing layer and wake, the spanwise vorticity is calculated and shown in the center of the frames of Fig. 9. The vortices are formed in $y \approx 0$, that corresponds to the upper edge of the plates. Clearly the thicker plate presents lower vorticity in the center of the vortices (less negative), but it forms larger vortices.

In both cases there is vortex pairing, but while the thicker plate has some vortices that does not pair with others, in the 'default' thickness sometimes three vortices merge (as in the Fig. 9(a) at $x \approx 90$). Due to this behavior neither simulations has shown periodicity.

In Fig. 9 the resulting emitted sound can be visualized by the dilatation field $\nabla \vec{u}$. The sources of noise cannot be determined precisely, but the vortex pairing seems to be an origin of sound emission, it can be identified $x \approx 160$ and $x \approx 260$ as a sources for the default plate (Fig. 9(a)), and that corresponds to the moment when the line that connect both centers of the pair is parallel to the streamwise direction. The mechanism of the noise emission by the vortex pairing is

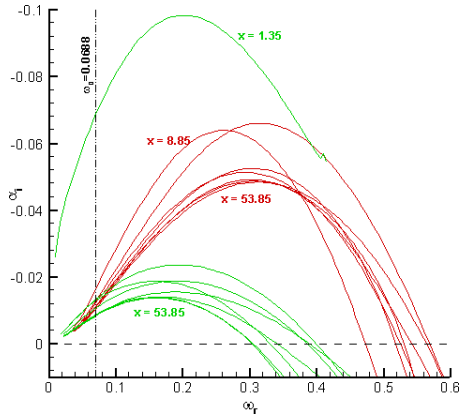

Figure 6. Spatial amplification rates for various x-positions behind the plate predicted by linear stability theory. 'Pure wake' case.

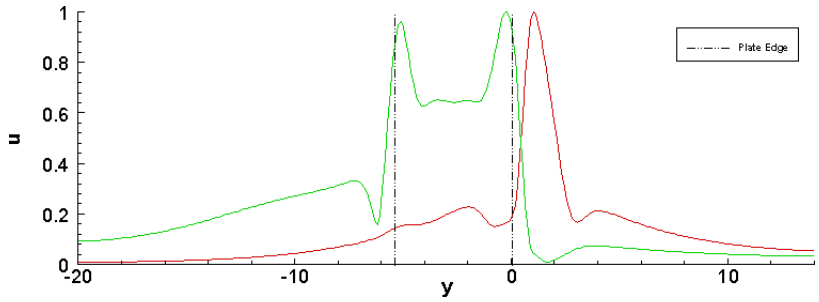

(a)

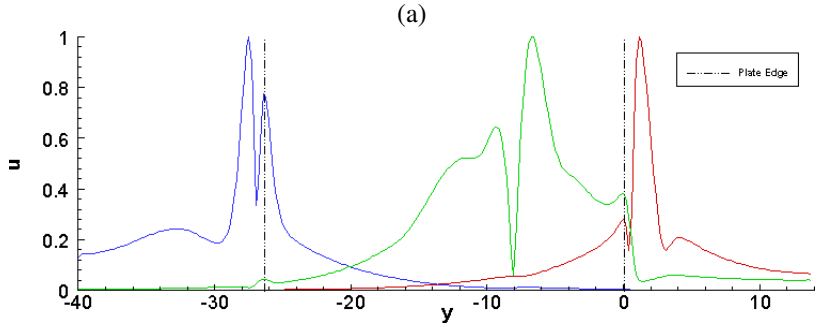

(b)

Figure 7. u' eigenfunctions at $x = 8.85$ for temporal amplification ($\alpha = \alpha_r = 0.2$). Shear layer mode in red, wake mode in green and upstream mode in blue. (a) 'Default' case. (b) 'Thicker' case.

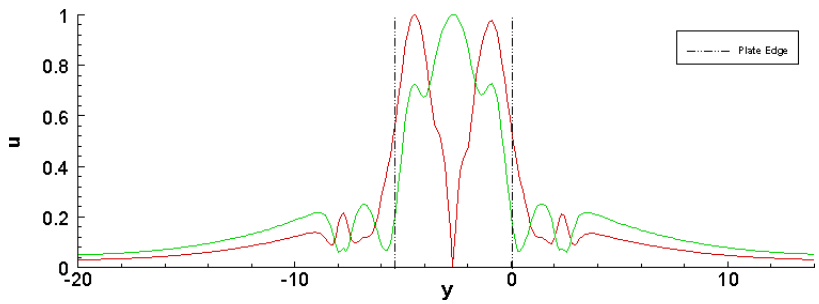

Figure 8. u' eigenfunctions at $x = 8.85$ for temporal amplification ($\alpha = \alpha_r = 0.2$). 'Pure wake' case.

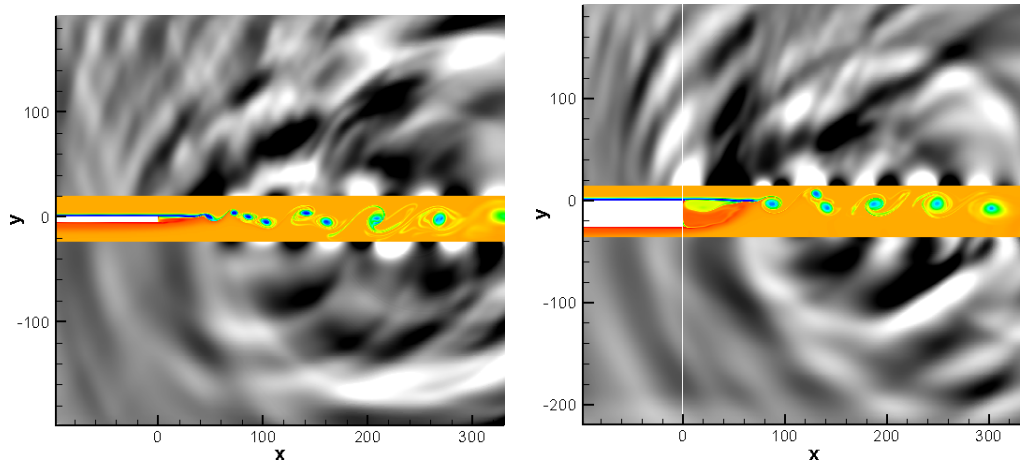

(a) (b)

Figure 9. Snapshot of the dilatation in a range of $\pm 3.10^{-4}$ and vorticity in a range of $[-0.35, 0.07]$. (a) 'Default' case. (b) 'Thicker' case.

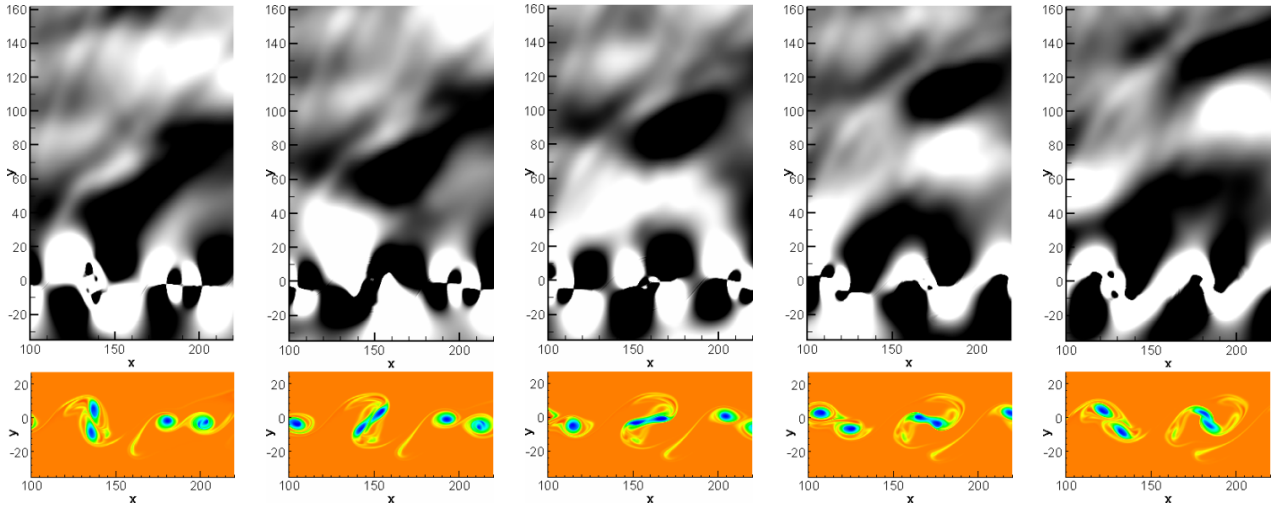

(a) (b) (c) (d) (e)

Figure 10. Noise emision by development of vortex pairing. The emission of a disturbance between frames (c) and (d) at $x \approx 160$ can be noted. The time between two consecutive frames is 0.2 of the fundamental period.

shown in Fig. 10. Since the simulation of the 'Thicker' case is less periodic and the x-position of vortex pairing varies, no position could be identified with the noise generated by the vortex pairing. On the other hand, in this simulation a source corresponding to the emission of vortices at $x \approx 40$ can be noted (Fig. 9(b)).

In both dilatation fields there are some reflections propagating upstream in the upper subdomains. These are reflections from oblique waves that are not damped well by the freestream boundary condition (see section 2.2). The reflected waves have small amplitudes, so it is believed that they did not alter the results significantly.

The results of the pure wake case is clearly a von Kármán vortex street, whose mechanism is different from the vortex pairing from a mixing layer. Therefore, besides the results from linear stability theory, no similarities could be observed between the simulations of the mixing layer/wake and the pure wake.

4.3 Spatial Amplification Rates

For the combination of mixing layer and wake, spatial amplification rates α_i calculated using DNS are compared to the ones found by LST. Only the greater value of the amplification rates for a given streamwise position found by linear stability theory is taken, since it is expected that the more amplified mode be the dominant one. The normal velocity v is used to obtain α_i from the results of DNS, as it is less associated to upstream propagating sound.

The modes are denoted as (h, k) with h and k being the multiple of fundamental frequency (ω_0) and the spanwise wavenumber, respectively. Although this is a two-dimensional study, it was chosen to keep the conventional notation, therefore $k = 0$ always.

As it can be seen in Fig. 11, for the fundamental frequency and its first higher harmonics (2,0) and (3,0) the amplifica-

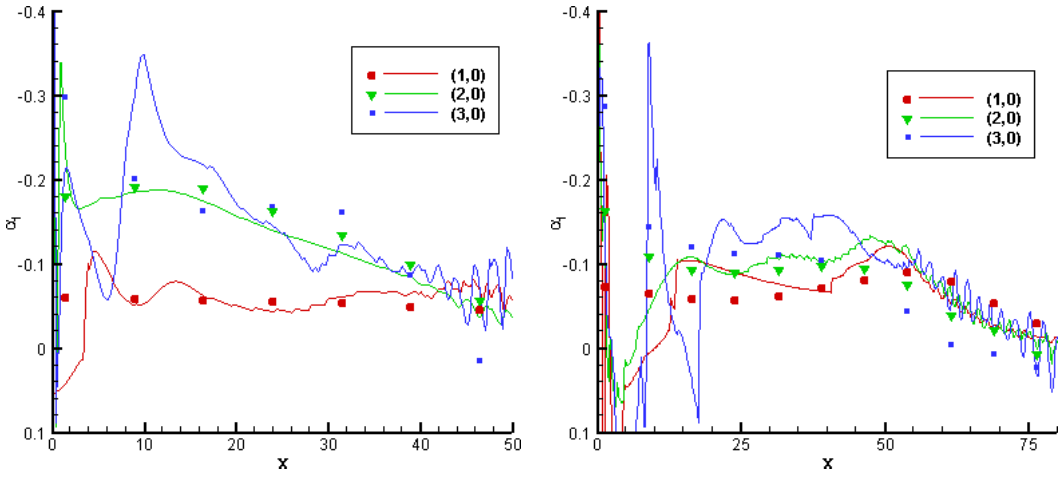

(a) (b)

Figure 11. Amplification rates of normal velocity v behind nozzle end, based on maximum amplitudes along y. Symbols denote results from linear stability theory. (a) 'Default' case. (b) 'Thicker' case.

tion rates agree quite well, especially for (1,0) and (2,0). The thicker plate shows worse agreement, this may be caused by the nature of the flow, for which the parallel approximation is worse. The same reason explains the high difference of the amplification rates near the plate. It was observed that the length of the region of great disagreement has a relation with the thickness of the plate, being about $x \approx 7$ for $t_K = 5.4$ and $x \approx 17$ for $t_K = 26.4$.

Further downstream the region is dominated by vortices, then the velocities begin to differ too much from the base flow of LST, v' saturates and it becomes difficult to calculate α_i by DNS, therefore it makes no sense to compare the results for greater x-positions.

4.4 Maximum Amplitudes

The maximum amplitudes of the perturbation of normal velocity are shown in Fig. 12. Fig. 12(a) corresponds to the thin plate with thickness $t_K = 0.15$ from the work of Babucke, Kloker, and Rist (2007b). Along the splitter plate $x \leq 0$, the values for the upper boundary layer are used.

In all cases the flow is dominated by the fundamental frequency and its integer multiples. In the region where the first vortex is generated (beetwen $x = 50$ and $x = 80$) some higher harmonics dominate for $t_K = 0.15$ ((3,0) and (2,0)) and $t_K = 5.4$ ((2,0) and (4,0)), while for $t_K = 26.4$ the fundamental frequency is dominant. This behavior can partly be explained by the amplification rates from linear stability theory, but it does not predict the growth for higher harmonics (greater than (4,0)), since the higher frequencies are due to non-linear generation. Downstream, where the pairing is developed ($x > 120$), the lower frequencies (1,0) and (2,0), in this order, are the dominant frequencies for all the simulations.

It can be seen for the thick plates that non-integer frequencies have greater amplitudes than for the thin plate in all regions of the flow, along the plate, near the plate edge and farther downstream. Near the thicker plate ($t_K = 26.4$) some low frequencies (lower than (0.22,0)) are dominant, and the higher amplitude occur for (0.094,0), this region corresponds to the region of "dead air" where there is recirculation of flow and the velocities are low.

It is probable that upstream travelling acoustic waves generate additional instability waves at the splitter plate. This may be one of the reasons that contributes to the non-periodicity of the flow.

4.5 Analysis of the Far-field

In order to evaluate the influence of the thickness of the trailing edge on the noise detected in the far-field an observer was placed at position $x = 195$ and $y \approx -121.8$.

Broadband noise is emitted instead of tonal noise known from the pure mixing layer (Colonius, Lele, and Moin, 1997) and the pure wake. The fluctuation of pressure for all the cases are similar, as it can be seen in Fig. 13, with a full spectrum with higher amplitudes near the fundamental frequency and decaying amplitudes for higher frequencies. For the thick plates ($t_K = 5.4$ and $t_K = 26.4$) the higher peak appears in the fundamental frequency, what does not occur for the thin plate. It can also be seen peaks in higher harmonics of the fundamental frequency ($\omega/\omega_0 = 2, 3, 4$) for all simulations. Yet a few differences can be observed:

- The amplitudes of fluctuations at low frequencies, $\omega/\omega_0 < 1$, is greater for the thicker plate ($t_K = 26.4$).
- For $\omega/\omega_0 = 4$ the amplitude is considerably higher for $t_K = 5.4$ (compared to $t_K = 0.15$ and $t_K = 26.4$).

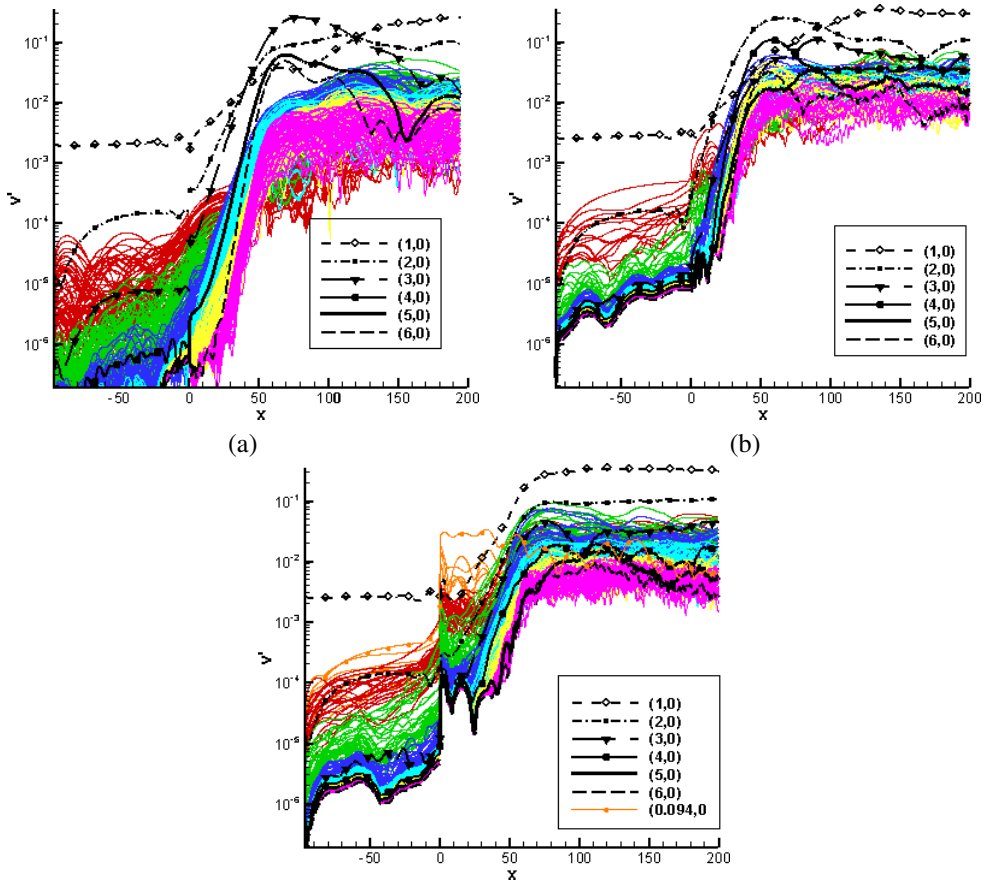

Figure 12. Maximum amplitude of the normal velocity fluctuation v' in the upper boundary layer $(x < 0)$ and behind the splitter plate $(x \geq 0)$. Integer harmonics are in black. Each other color represents non-integer harmonics, for (a) and (b) these are colored in red [(0,0)-(1,0)], green [(1,0)-(2,0)], dark blue [(2,0)-(3,0)], light blue [(3,0)-(4,0)], yellow [(4,0)-(5,0)] and purple [(5,0)-(6,0)], for (c) these are colored in orange [(0,0)-(0.22,0)], red [(0.22,0)-(1,0)] and the same colors as the others. (a) 'Thin plate' case. (b) 'Default' case. (c) 'Thicker' case.

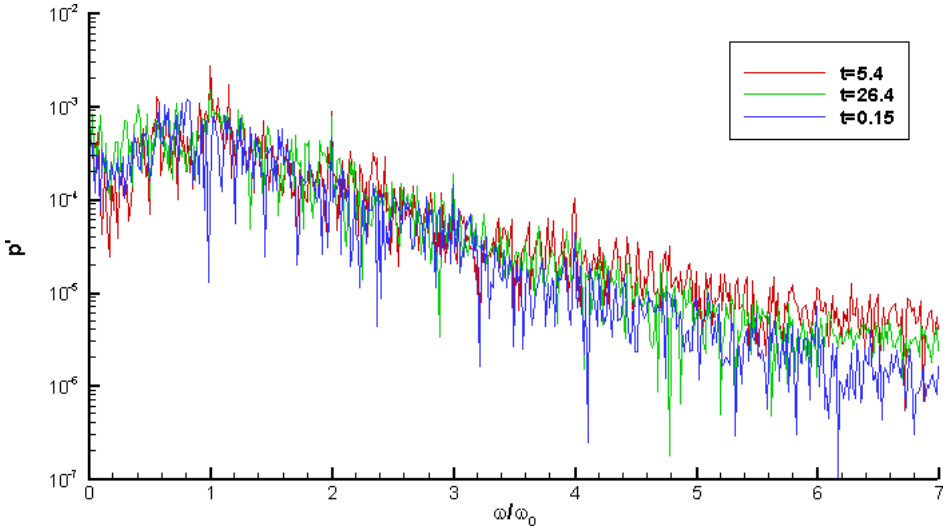

Figure 13. Amplitude spectrum of the acoustic pressure relative to the observer's position ($x = 195$ and $y \approx -121.8$).

- At the region of high frequencies ($\omega/\omega_0 > 5$), $t_K = 5.4$ presents the higher amplitudes of fluctuations, followed by $t_K = 26.4$ and $t_K = 0.15$ presenting the lower amplitudes.

All these characteristics can be related to Fig. 12, of maximum aplitudes of v':

- The thicker plate ($t_K = 26.4$) has high amplitudes of low frequencies near the plate.
- For $t_K = 5.4$, (4,0) is an important harmonic in the region of $40 < x < 70$.
- Further downstream $t_K = 5.4$ presents the higher amplitudes of v' for high frequencies, followed by $t_K = 26.4$ and $t_K = 0.15$ presenting the lower amplitudes.

Based on these relations it is observed that the whole the domain may be relevant to the far-field noise, therefore reaffirming that aeroacoustic simulation demands a large computational domain.

5. CONCLUSIONS

The nozzle end of an isothermal jet with Mach numbers $Ma_I = 0.8$ and $Ma_{II} = 0.2$ has been simulated using two-dimensional DNS. The nozzle end wall was simulated by thick splitter plates and the results were compared with thin splitter plate. A combination of wake and mixing layer was obtained, with mixing layer phenomena being dominant. However the flow differs considerably from a pure mixing layer, being non-periodic and with unique mechanisms of vortex emission. A pure wake was simulated in search for similarities, but the only similarities obtained came from linear stability theory.

Linear stability theory has shown good agreement with the DNS simulations for the first integer multiples of the fundamental frequency. But due to large amplitudes, non-linear mechanisms produced a wide spectrum of disturbances, with peaks at multiples of the fundamental frequency. The many spectra of the acoustic pressure were very similar, but some differences could be noted and it was possible to interrelate them with the maximum amplitudes of normal velocity fluctuations. These results also show the importance of a large domain for acoustic simulations.

Further work could be done on a wider range of thickness, three-dimensional geometries and the improvement of the grid generation in order to simulate other forms of plate, for example a trapezoidal splitter plate. This kind of study can also lead to development of actuators for noise reduction.

6. REFERENCES

Babucke A., Linn J., Kloker M.J., and Rist U. Direct numerical simulation of shear flow phenomena on parallel vector computers. *High performance computing on vector systems: Proceedings of the High Performance Computing Center Stuttgart, 2005*, pages 229–247, 2006.

Babucke A., Kloker M.J., and Rist U. Direct Numerical Simulation of a Serrated Nozzle End for Jet-Noise Reduction. *High Performance Computing in Science and Engineering'07: Transactions of the High Performance Computing Center, Stuttgart (HLRS) 2007*, pages 319–337, 2007a.

Babucke A., Kloker M.J., and Rist U. Numerical Investigation of Flow-Induced Noise Generation at the Nozzle End of Jet Engines. *Notes on Numerical Fluid Mechanics and Multidisciplinary Design*, 96:413–420, 2007b.

Babucke A., Kloker M.J., and Rist U. DNS of a plane mixing layer for the investigation of sound generation mechanisms. *Computers and Fluids*, 37(4):360–368, 2008.

Bogey C., Bailly C., and Juve D. Numerical simulation of sound generated by vortex pairing in a mixing layer. *AIAA Journal*, 38(12):2210–2218, 2000.

Colonius T., Lele S., and Moin P. Boundary conditions for direct computation of aerodynamic sound generation. *AIAA Journal*, 31(9):1574–1582, 1993.

Colonius T., Lele S.K., and Moin P. Sound generation in a mixing layer. *Journal of Fluid Mechanics*, 330:375–409, 1997.

Freund J.B. Noise sources in a low-Reynolds-number turbulent jet at Mach 0.9. *Journal of Fluid Mechanics*, 438:277–305, 2001.

Giles M. Nonreflecting boundary conditions for Euler equation calculations. *AIAA Journal*, 28(12):2050–2058, 1990.

Kloker M.J. A Robust High-Resolution Split-Type Compact FD Scheme for Spatial Direct Numerical Simulation of Boundary-Layer Transition. *Applied Scientific Research*, 59(4):353–377, 1997.

Zhuang M. and Dimotakis P.E. Instability of wake-dominated compressible mixing layers. *Physics of Fluids*, 7(10): 2489–2495, 1995.

7. RESPONSIBILITY NOTICE

The authors are the only responsible for the printed material included in this paper.